IOSR Journal of Applied Physics (IOSR-JAP)
e-ISSN: 2278-4861.Volume 9, Issue 4 Ver. II (Jul. – Aug. 2017), PP 64-70
www.iosrjournals.org

Single Crystal Q-Band EPR Studies of Mn (II) Doped Ammonium Catena - Di-μ-Chromatodiammine Cadmium (II)

K. Vijayaraj[1], A. Jawahar[1], R. Anantharam[2], M. Kumara Dhas[3*]
[1] *Department of Chemistry, NMSSVN College, Nagamalai, Madurai-625019, Tamilnadu, India*
[2]*Department, of Chemistry, ANJA College, Sivakasi, Tamilnadu, India*
[3]*Department of Physics, Mahendra Arts and Science College, Kalippatti, Namakkal-637501, Tamilnadu, India*
Corresponding Author: nmdhas@gmail.com

Abstract : *The Single crystal Q-band EPR studies of Mn (II) doped ammonium catena-di-μ-chromatodiammine cadmium (II), $(NH_4)_2[Cd(NH_3)_2(CrO_4)_2]$ has been carried out at 300 K. Although three magnetic sites are observed, the angular variation for only two sites could be studied. It reveals that the paramagnetic impurities, Mn(II), occupy the substitutional sites in the host Cd (II) lattice. Due to the non-first order nature of the spectrum, all the work had to be carried out at Q-band frequency. The spin Hamiltonian parameters obtained for site 1 are* $g_{II} = 1.986$, $g_{\perp} = 1.979$, $A_{II} = -78.1$, $A_{\perp} = -80.3$, *D = 1109.8 G, E = -231.7 G, a = 10 G and for site 2 are* $g_{II} = 1.975$, $g_{\perp} = 1.978$, $A_{II} = -79.5$, $A_{\perp} = -78.4$, *D = 784.9 G, E = -149.0 G (where A is in units of 10^{-4} cm^{-1}), forbidden transitions corresponding to $\Delta m_I = \pm 1$ and ± 2 are observed for a number of orientations and their positions have been calculated by perturbation theory taking into account, the second order admixtures due to cross terms in D and hyperfine coupling constant A.*

Keywords: *Angular variation, Electron spin resonance, hyperfine coupling, paramagnetic ions, single crystal,*

I. Introduction

The Electron Paramagnetic Resonance (EPR) of Mn(II) has been widely used to probe site symmetry [1-5], phase transition [6-8], host spin-lattice relaxation [9-11] and the effect of uniaxial stress on crystals [12]. Mn(II) with high spin d^5 configuration, is selected as EPR probe because of its long spin-lattice relaxation time and the fact that the magnitude and orientation of the zero-field tensor, are highly sensitive to the strength and symmetry of the crystal [13-18]. Hence, EPR of Mn(II) in different crystal field environments viz., tetrahedral, cubic or octahedral coordination has been studied. An interesting observation of unusually large D value and intense forbidden hyperfine transitions has been reported for EPR of Mn(II) in ammonium halides [19,20]. Mn(II) was assumed to occupy interstitial position [21-24]. It is surrounded by four Cl^- ions and two water molecules at relatively short distances than Cl^- ions resulting in tetragonally compressed geometry [25].

The electron paramagnetic resonance study of Mn^{2+} ion doped in tetraaquabis(hydrogen maleato)cadmium(II) single crystal indicates that Mn^{2+} ion has entered the lattice interstitially and its location has been identified by the atomic coordinates of host lattice [26]. S. Ravi etal, reported the electron paramagnetic resonance study on manganese doped tetrathiureacopper(I) chloride single crystal, which reveals that the manganese present in tetravalent state in interstitial position with isotropic g and A value [27]. In the EPR studies of Mn(II) doped zinc potassium phosphate hexahydrate, the distortion axis for the substituent site has been identified as one of the Zn-O directions in the lattice and confirms that the impurity has entered the lattice substitutionly [28]. The XRD and EPR spectroscopy studies of Manganese-doped $ZnAl_2O_4$ (gahnite) samples show pure gahnite has normal spinel structure, while Mn-doping induced the appearance of partial inverse spinel structure with Mn^{2+} ions residing on both tetrahedral and octahedral cation sites [29]. Electron paramagnetic resonance study of Mn^{2+} ion-doped Tetraaquabis(hydrogen maleato)cadmium(II) single crystal indicates Mn^{2+} ion has orthorhombic symmetry, Mn^{2+} ion has entered the lattice interstitially [30]. EPR spectroscopic studies confirmed the presence of both Mn^{2+} and Mn^{4+} ions in zinc pyrophosphate. The Mn^{2+} at Zn^{2+} site having octahedral coordination of oxygen whereas the presence of an EPR signal attributed to Mn^{4+} at Zn^{2+} site having considerably lower symmetry due to the presence of extra interstitial oxygen ions or due to the substitution of manganese at distorted 5-coordinated zinc site [31]. Ram Kripal et.al observed one interstitial site for Mn^{2+} ions doped in sarcosinium oxalate monohydrate (SOM) single crystal at liquid nitrogen temperature (LNT) using Electron paramagnetic resonance study [32]. Muhammed Acikgoz et.al analyzed the zero-field splitting parameters of Mn^{2+} ions doped into yttrium aluminum borate $YAl_3(BO_3)_4$ single crystal, replacement of the Mn^{2+} for Al^{3+} induces a sizable lattice distortion, which gives rise to a large D value. The result also indicates the zero-field splitting depends linearly on the angular distortion of the ligands around Mn^{2+} doped into $YAl_3(BO_3)_4$ [33]. Ram Kripal et.al. reported the EPR and optical absorption studies of Mn^{2+} doped

ammonium tartrate, EPR study reveals that the Mn^{2+} ions are expected to occupy distorted octahedral substitutional sites and the optical studies show the rhombic distortion in the lattice [34]. K. Ravindranadh et.al investigated the optical and structural properties of undoped and Mn^{2+} doped Ca–Li hydroxyapatite nanopowders using mechanochemical synthesis, which reveals the doped Mn^{2+} enter into the host material as distorted octahedral site [35]. In an attempt to understand the unusually high D value and the forbidden hyperfine transitions, a search for suitable diamagnetic host lattices, where the central metal ions are axially compressed, has been carried out. Also, Mn(II) can be substitutionaly incorporated in it. The compound, $[(NH_4)_2[Cd(NH_3)_2(CrO_4)_2]$ (hereafter referred to as ACDC has been selected because of the that the Cd(II) is present in tetragonally compressed geometry [25]. It was also revealed by EPR of Cu (II) doped ACDC to exhibit inverse spectra i.e., $g_\perp > g_{||}$ characteristic of tetragonal compression [36]. Preliminary investigation of the EPR spectra of Mn(II) doped ACDC at X-band showed it to be highly complicated. It is because of the fact the spectra at low field region do not satisfy the condition $H_z >> H_{ss}$. Due to the off-diagonal elements in H_{ss}, many forbidden hyperfine lines occur. Moreover, the microwave quantum at X-band is not sufficient to connect some of the energy levels even at zero field. So, EPR of Mn(II)-doped ACDC is studied at Q-band frequency and reported here.

II. Materials And Methods

Experimental

Single crystals of Mn(II) doped $(NH_4)_2[Cd(NH_3)_2(CrO_4)_2]$ (hereafter referred to as MCAC) were prepared by slow evapouration of a mixture of solution of $CdSO_4.4H_2O$ containing one percent of $MnSO_4$ in concentrated ammonia and ammonium dichromate in the molar ratio of 1:2:1[25]. Pale yellow crystals of MCAC, suitable for single crystal EPR studies were obtained within three days. EPR spectra were recorded at Q-band frequencies on a Varian E-112 EPR spectrometer having a 100 KHz field modulation and phase sensitive detection to obtain the first derivative EPR signal. DPPH with a g-value of 2.0036 was used as an internal field marker for g-factor calculations. Angular variation studies were made by rotating the crystal about the three mutually orthogonal axes, a*, b and c (for every 10° rotation) c is perpendicular to the crystallographic *a*- and *b*- *axes.*

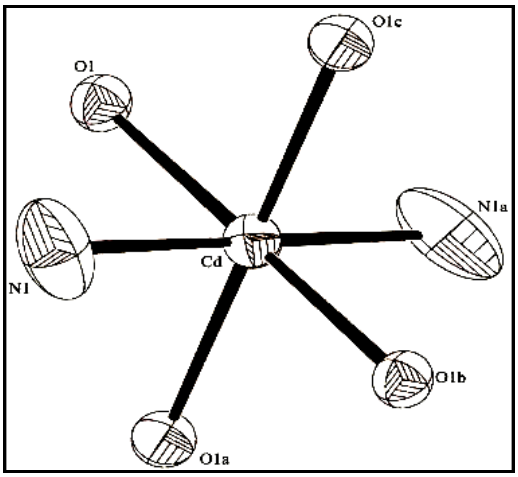

Fig. 1 The Ortep diagram for the chromophore $Cd(NH_3)_2O_4$. Four equivalent oxygen atoms from CrO_4 polyhdedra and two nitrogen atoms from two ammonia molecules surround the central cadmium in the equatorial and axial positions respectively.

Crystal structure of $(NH_4)_2[Cd(NH_3)_2(CrO_4)_2]$

The crystal structure of the host lattice has been reported to exhibit phase transition [25]. At and above 300 K, it exists as monoclinic space group C2/m with cell dimensions, a = 12.8380(1), b = 6.0308(6), c = 7.5890(6) Å , β = 110.15(14)° and Z = 2. However, below 300 K, it changes to a triclinic space group P1 with cell dimensions, a = 6.0210(4), b= 7.0363(4), c = 7.714(8) Å, α = 106.802(18), β = 93.032(12), γ = 114.08(11)° and Z = 1. The crystal lattice consists of Cd(II) octahedral. Figure 1 shows the schematic diagram of the chromophore $Cd(NH_3)_2O_4$. The central Cd(II) is surrounded by four equivalent oxygen atoms (Cd-O = 2.368(2) Å) at the corners of a square (*ab* plane) from four different CrO_4 polyhedra. Two nitrogen of ammonia molecules occupy the axial positions along the c-axis (Cd-N = 2.194(3) Å). The tetragonality, defined as the ratio of mean in-plane distance to the mean out-of-plane distance is 1.043 and it deviates from unity, expected for an ideal octahedron, indicating the geometry around Cd(II) to be axially compressed octrahedron. The projection of the crystal structure down c- and b*- axes are shown in Figure 2. It is evident that the two CdN_2O_4 chromophores are similarly oriented and equivalent. The Cd(II) octahedral are linked by pairs of tetrahedral chromate groups to form a chain along b axis.

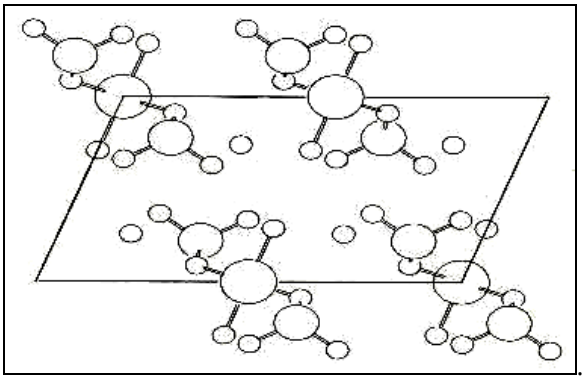

Fig. 2 The crystal structure projection of down a* and b-axes. A chain b- axis is formed by the linkage of pair of tetrahedral line

III. Results And Discussion

The In the absence of an external magnetic field, the ground state $^6S_{5/2}$ ion splits into three Kramers doublets corresponding to $|\pm 1/2\rangle, |\pm 3/2\rangle$ and $|\pm 5/2\rangle$ due to spin-spin interaction. The energy gap between the ground Kramers doublet and the first excited doublet is 2D and that between the second and third doublets is 4D, where D is the zero-field splitting. These three Kramers doublets are further split in the presence of an applied magnetic field to give rise to six non-degenerate levels. Hence, in EPR one should expect five equally spaced resonances, corresponding to five allowed ΔMs = ±1 transitions. Each of these five lines is split further into a sextet, due to hyperfine interaction (I = 5/2) and hence, one can expect a 30-line pattern per crystal site. Due to other zero-field terms like *a* and *F* and due to second order effects, these five groups and the sextets in each group are not equally speed [37-39].

Single crystal EPR spectra showed more than 60 lines in all the three planes. Typical single crystal spectra of MCAC in the ac* and bc* planes are shown in Figures 3 and 4. It clearly indicates the presence of three distinct magnetic sites. The EPR spectra observed could be fitted to the following spin Hamiltonian.

$$H = g\beta BS + ASI + D\left[S_z^2 - \left(1/3\right)S(S+1)\right] + E\left(S_x^2 - S_y^2\right)\left(\frac{1}{6}\right)a\left[S_\alpha^4 + S_\beta^4 + S_\gamma^4 - \left(\frac{1}{5}\right)S(S+1)(3S^2+S-1)\right] \quad (1)$$

Where, the first term represents the Zeeman energy and the second term the hyperfine interaction. The third and fourth terms represent the axial component of the zero-field splitting and the cubic field respectively. Here α, β, γ are the three orthogonal axes of the cubic crystalline field.

The angular variations of fine structure lines for sites 1 and 2 are given in Figure 5. It is evident that the two sites 1 and 2 are misaligned by about an angle of 90°. The angular variations follow (3 $\cos^2\theta$-1) dependence. The spread of the spectra is maximum at θ = 0° and starts decreasing as θ increasing and nearly collapses at θ = 54˚.44′, where (3 $\cos^2\theta$-1) becomes zero. As θ increases further (3 $\cos^2\theta$-1) becomes negative and hence fine structure lines cross each other. These angular variations of the fine structure lines could be fitted to the spin Hamiltonian (1). Correct to second order in perturbation, the line positions for the give fine structure transitions are given by

$$g\beta B\left(\pm\frac{5}{2}\leftrightarrow\pm\frac{3}{2}\right) = g\beta B_0 \mp 4a_0 - \left(32a_1^2 - 16a_2^2\right)/g\beta B_0$$

$$g\beta B\left(\pm\frac{3}{2}\leftrightarrow\pm\frac{1}{2}\right) = g\beta B_0 \mp 2a_0 + \left(4a_1^2 - 20a_2^2\right)/g\beta B_0$$

$$g\beta B\left(\pm\frac{1}{2}\leftrightarrow\mp\frac{1}{2}\right) = \left(16a_1^2 - 32a_2^2\right)/g\beta B_0 \quad (2)$$

Here,

$$2a_0 = D(3n^2-1) + 3E(l^2-m^2)$$

$$a_1^2 = D^2n^2\left(1-n^2\right) + E^2\left[(l-n^2) - \left(l^2-m^2\right)^2\right] - 2DEn^2\left(l^2-m^2\right)$$

$$16a_2^2 = D^2\left(1-n^2\right)^2 + E^2\left[4n^2 + \left(l^2-m^2\right)^2\right] + 2DE\left(n^2+l\right)\left(l^2-m^2\right) \quad (3)$$

Where, 1, m, n are the direction cosines of the magnetic field with respect to the x, y and z axes. Due to the complexity of overlap of the fine structure lines of sites 3, only the angular variation of 5/2 ↔ 3/2 transition could be followed and it is found to be almost isotropic.

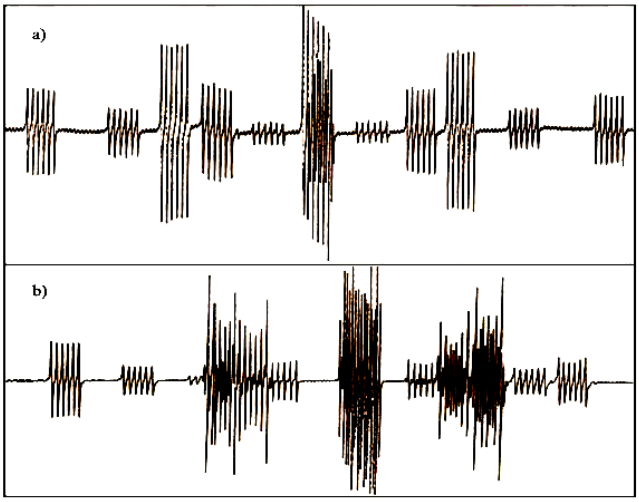

Fig. 3 Single crystal Q-band EPR spectra of MCAC for ac* plane (a) B ‖ a and (b) B ‖ c*

TABLE 1. Spin Hamiltonian parameters for MCAC and related systems.

Compound	g	G	A	A	D	E	Ref.
MCAC site1 site2	1.979 1.975	1.986 1.978	-78.1 -80.3	-79.5 -78.4	1048.7 1109.7	-216.8 -149.0	This Work
Mn(II)_NH_4Cl	2.002	.001	90.2		-1384.2		[40]
Mn(II)_$NH_4$1	2.000		82.6		-1505.4		[41]
Mn(II)_$RbMgBr_3$	2.003		79.0		±983.0		[42]
Mn(II)_$CsMgBr_3$	2.004		77.0		±950.0		[42]
Mn(II)_SAIC	2.001		83.5		-790.0	-80.4	[42]
Mn(II)_$(NH_2)_2CO.NH_4Cl$			86.9	85.2	744.7 712.2 736.5	-127.1 -160.8 -111.2	[43] [43] [43]

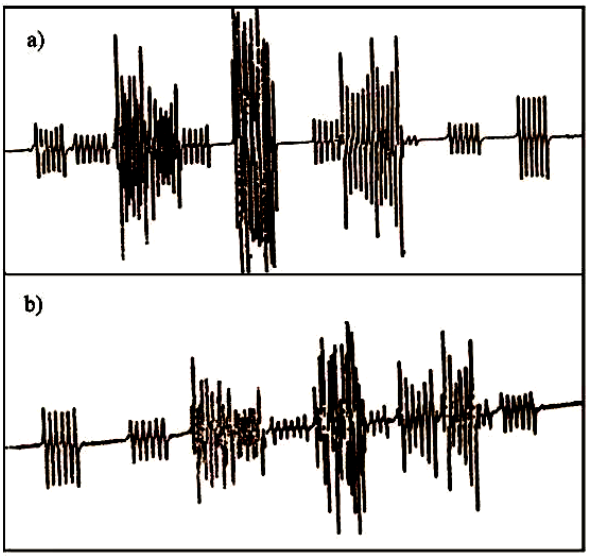

Fig. 4 Typical single crystal Q-band EPR spectra of MCAC for bc* (a) B || b and (b) B || c*

Table 1 reveals that the g factor of MCAC is isotropic, as expected for a $^6S_{5/2}$ ground state. The hyperfine tensor for Mn(II) ion is also generally found to be isotropic. To calculate the line positions for allowed hyperfine transitions, M ↔ M-1, ΔM = 0, the following terms were added to the values of B, given by eq (4).

$$- A_{II} m - \left(\frac{A_{\perp}^2}{2 B_0} \right) \left[I(I+1) - m^2 + m(2M - 1) \right] \tag{4}$$

Where, M and *m* are electron spin and nuclear spin quantum numbers respectively. The second order term in A⊥ causes small differences in the spacing of the hyperfine lines. Using the above equation, the spacing of successive lines parallel to the symmetry axis may be readily found to be

$$A_{II} + \left(\frac{A_{\perp}^2}{B_0} \right) (M - m) \tag{5}$$

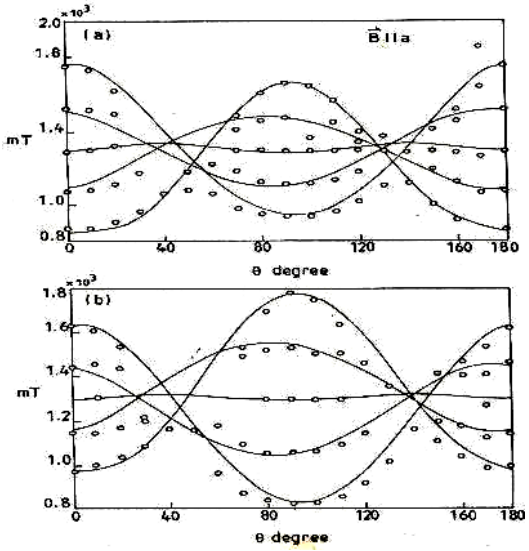

Fig. 5 Calcualted (−) angular variations of the fine structure lines of MCAC in ac* plane for sites1 and 2. Experimental angular variations are represented by (a) for site 1 and (b) site 2. For both sites, the calculated and experimental values coincide well

For perpendicular orientations, the line positions are given by

$$A_{\perp} + \left[\left(A_{II}^2 + A_{\perp}^2 \right) / 2 B_0 \right] (M - m) \tag{6}$$

The $A_{\parallel}$ given in Table 1 is the average value of the hyperfine splitting in the five fine structure groups of the spectrum obtained for the maximum spread (θ = 0, Figure. 3a). Similarly A⊥, was calculated from the 90° spectrum. (Figure 3b). Using the above equations and least-squares method, the spin Hamiltonian parameters D and E for sites 1 and 2 were calculated by considering the spectra recorded at various orientations in the *ac** plane. The calculated spin Hamiltonian parameters, along with those of other related systems are given in Table 1. Using the values of D and E given in Table 1, the angular variations of zero-field transitions for site 1 and 2 were simulated and are shown in Figure 5 where good agreement between calculated and the experimental angular variation of the fine structure transitions are seen.

Also, based on the direction cosines of the metal-ligand bonds and the spin Hamiltonian parameters of sites 1 and 2 listed in Table 1, the angular variation of the fine structure lines can be successfully simulated (as shown in Figure 5). The simulation could be successful only if the distortion axis for one site is assumed to be along the Cd-N bond and for another site, orthogonal to this direction. This also supports the fact that both the Mn(II) sites are subsitutionally incorporated in the Cd(II) lattice and are out of phase by 90°. However, the crystal structure data revealed that there are two molecules in the unit cell. Both of them are magnetically equivalent as seen from their similar spatial disposition in the unit cell packing diagram[25]. Hence, only one site, corresponding to the substitutional occupancies of Mn(II) in Cd(II) sites is expected for all the three planes. Therefore, the presence of the two substitutional sites may be attributed to the growth of crystals in two orthogonal directions *i.e.,* one along the distortion axis and the other, distortion axis perpendicular to it. The relatively large magnitudes of D and E values for the substitutional sites 1 and 2, listed in Table 1 along with the related systems reveal that the axial distortion in MnO_4N_2 is strong. However, the large difference in the values of D for sites 1 and 2 clearly confirm to be out of phase with each other (*vide supra*).

Relative signs of D and A

The signs of the zero field parameters given in Table 1**,** are relative to the sign of the hyperfine coupling constant, A of Mn(II). These relative sign were obtained from the second order effects by comparing the

separation between the hyperfine components of the various fine-structure transitions. If A and D are of the same sign, the separation of the hyperfine lines will be larger at low fields than at the high fields, whereas, the converse is true when A and D are of the opposite sign. Analysis of the spectra reveals that the separations of the sextets increase towards high fields and hence, D/A is negative by theoretical restricted Hatree-Fock calculations, it is shown that the isotropic coupling constant for high spin Mn(II) complexes arises via the polarization of the inners electrons and it is negative in sign [43]. Thus, the negative sign for A implies that D is positive. Only a negative sign for E leads to the successful simulation of the angular variation (Figure 5).

Forbidden Transitions

Apart from normal sextet hyperfine features on each of the fine structure transitions, in many orientations forbidden transitions corresponding to $\Delta M_I = \pm 1$ and ± 2 have also been observed. These transitions borrow intensity from the normal transitions thereby imparting curious intensity distributions on them. Second order terms in hyperfine, quadrupolar and nuclear Zeeman Hamiltonians can give rise to these transitions by bringing about an admixture of the various m_I levels. The admixture coefficients are proportional to the magnitude of these terms. Perturbation theory correct to second order predict the relative intensities of these transitions to be $(Q/A)^2$ or $(g_n\beta_n B/A)^2$ or $(A/g\beta B)^2$ for a quadrupole dominated, or nuclear Zeeman dominated or hyperfine Hamiltonian respectively.

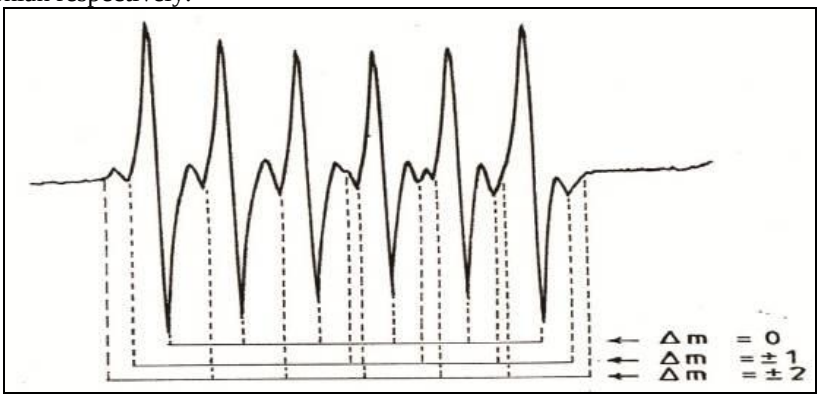

Fig. 6 Typical example of forbidden transitions, ΔMs = ± 1 and ± 2, shown for the fine structure transition for the sites 1 and 2.

Q-band spectra of MCAC exhibit forbidden transitions at many orientations and the normal transitions have approximately similar intensity. The above relations however predict very low intensities for the forbidden transitions. Besides $\Delta M_I = \pm 2$ transitions can be brought about only by an orthorhombic Q-tensor, correct to second order. Third order perturbation in the hyperfine interaction H_{HF} and the nuclear Zeeman term H_{NZ} which will require wave function correct to second order can bring about $\Delta M_I = \pm 2$ transitions. But, these transitions will be much lower in intensity. We, therefore, resort to the procedure of Bleanely and Rubins [44], where second order admixtures due to cross terms in A and D, correct to third order in energy predict intense forbidden transitions. Using the equivalent operator formalism, it has been derived that forbidden transitions with $\Delta M_I = \pm 1$ will have intensities given by

$$\left(\frac{3DSin\ 2\theta}{4g\beta B}\right)^2\left[1+\frac{S(S+1)}{3m_s(m_s-1)}\right]^2\left[I(I+1)-m_I^2+m_I\right] \tag{7}$$

Where, θ is the angle between D_{zz} and B, and for $\left|m_s, m_I \pm 1\right\rangle \leftrightarrow \left|m_{s-1}, m_I \pm 1\right\rangle$ transitions, it is given by

$$\left\{\left(\frac{1}{2}\right)\left(3D\sin\frac{2\theta}{4g\beta B}\right)^2\left[1+\frac{S(S+1)}{3m_s(m_s-1)}\right]^2 \pm \left[\frac{3DASin^2\theta}{16(g\beta B)^2}\right]\left[1+\frac{S(S+1)}{3m_s(m_s-1)}\right]\right\}^2 \left(I^2-m_I^2\right)\left[(I+1)-m_I^2\right] \tag{8}$$

The given expression for the state $\left|m_s, m_I\right\rangle$ due to the hyperfine terms is given by

$$Am_sm_I+m_I\left(\frac{A^2}{2g\beta B}\right)\left[m_S^2-S(S+1)\right]+m_s\left(\frac{A^2}{2g\beta B}\right)\left[I(I+1)-m_I^2\right]+\left(\frac{D\sin^2\theta}{4g\beta B}\right)^2\left(\frac{2Am_I}{m_s}\right)\left\{\left[m_s^2-S(S+1)\right]^2\right\}+$$

$$\left(\frac{D\sin^2\theta}{4g\beta B}\right)^2\left(2Am_Im_s\right)\left[2m_s^2+1-2S(S+1)\right] \tag{9}$$

Which includes important third order terms, arising from the cross terms between A and D, besides all second order terms. Using eq.(4)-(6), the position and intensities of the forbidden lines for a number of orientations have been calculated. In this calculation, the line positions of the forbidden transitions could be satisfactorily calculated, even without including the E-term and it is shown for a typical orientation in Figure 6. However, the prediction of intensities has not been good and it is somewhat not unexpected in view of the limitation of perturbation theory.

IV. Conclusion

Single crystal Q-band EPR studies of MCAC has been carried out at room temperature. Angular variation studies suggest that the two sites are substitutionally incorporated in the host Cd(II) lattice. The distortion axis of one of the substitutional sites has been observed to be along the Mn-N bond direction and for the other site, it is orthogonal to it. Forbidden transitions, corresponding to observed for a number of orientations and their positions were analysised using perturbation theory.

Acknowledgements

The authors K. Vijayaraj, and A. Jawahar, thank the management of NMSSVN College for encouragement and permission to carry out this work.

References

[1] R. Murugesan, V.S. Xavier Anthonisamy, S. Subramanian, Spectrochim. Acta. Part A, 49 (1993) 1801-1807.
[2] V.S Xavier Anthonisamy, D. Pathinettam Padiyan, R. Murugesan, Mol. Phys.94 (1998), 275-281.
[3] A. Milton Franklin Benial, V. Ramakrishnan, R. Murugesan Spectrochim. Acta. Part A, 55 (1999) 2573-2577.
[4] R. Murugesan, S. Subramaniyan, Mol.Phys. 52(1984) 281-288.
[5] Ch. Linga Raju, N.O. Gopal , K.V. Narasimhulu, J. Lakshmana Rao, B.C Venkata Reddy, Spectrochim. Acta. Part A, 61 (2005) 2181-2187.
[6] Ram Kripal, Vishal Mishra, Solid State Commun. 133 (2005) 23-28.
[7] S. Pal, R. Samata, A.K. Pal J. Phys. Soc. Jpn. 65 (1996) 647-648.
[8] A. Ozarowski, B.R. McGarvey, Inorg.Chem. 28 (1989) 2262-2266.
[9] T. Jeyabalan, P. Sami, A. Shanmugasundaram, R. Murugesan, Spectrochim. Acta. Part A, 55 (1999) 2187-2193.
[10] V.S. Xavier Anthonisamy, M. Velayutham, R. Murugesan, Physica B 263 (1999) 13-19.
[11] R. Murugesn, A. Thamaraichelvan, A. Milton Franklin, V.Ramakirshnan, Mol. Phys. 79 (1993) 663-672.
[12] E. Larson, A. Haddy, N.L. Kirk, R.H. Sands, W.E. Hatfiled, V.L Percorara, J. Am. Chem. Soc., 114 (1992) 6263-6265.
[13] V.S. xavier Anthonisamy, R. Murugesan, Mol. Phys. 93 (1998) 6.
[14] K. Velavan, R. Venkatesan, P. sambasive Rao, J. Phys. Chem. Solids, 66 (2005) 876-881.
[15] Vijay Singh, R. P. S. Chakradhar, J. L. Rao, S. J. Dhoble, S. H. Kim , J. Electron. Mater., 43 (2014) 4041–4047.
[16] Vijay Singh, G. Sivaramaiah, J.L. Rao, S.H. Kim, J. Lumin.,157 (2015) 74–81.
[17] B. Jaya Raja, M. Rajesh Yadav, V. Pushpa Manjari, B. Babu, Ch. Rama Krishna, R.V.S.S.N. Ravikumar, J. Mol. Struct., 1076 (2014) 461–467.
[18] Atul K. Gupta, Ram Kripal, Spectrochim. Acta. Part A, 96 (2012) 626–631.
[19] V. Lupei, A. Lupei, F. Domsa, J. Magn. Reson. 19 (1975) 337-344.
[20] Y. Li, X. Kuang, A. Mao, H. Li, R. Chai, Chem. Phys. Lett., 487 (2010) 307–311.
[21] R. Kripal, S. D. Pandey, Physica B, 444 (2014) 14–20.
[22] P. Aleshkevych, J. Fink-Finowicki, M. Gutowski, H. Szymczak, J. Magn. Reson., Ser A, 205 (2010) 69–74.
[23] S. K. Misra, S. Diehl, D. Tipikin, J. H. Freed, J. Magn. Reson., Ser A, 205 (2010) 14–22.
[24] R. Kripal, M. Singh, Chem. Phys. Lett., 610 (2014) 98–102.
[25] H.Headlam, M.A. Hitchman, H. Stratmeir, J.M.M. Smits, P.T. Beurskens, E.de Boer, G. Janssen, B.M. Gatehouse, G.B. Deacon, G.N. Ward, M.J. Riley, D. Wang, Inorg. Chem. 34 (1995) 5516-5523.
[26] Somasundaram Ramachitra, Ramesh Hema, Premkumar Muthuausteria, Krishnan Parthipan, J. Mol. Struct. 1058 (2014) 173-180.
[27] S. Ravi, P. Subramanian, Spectrochim. Acta. Part A, 67 (2007) 1150-1152.
[28] H. Anandalakshmi, I. Sougandi,K. Velavan, R. Venkatesan, P.S. Rao - Spectrochim. Acta. Part A, 60 (2004) 2661-2666.
[29] J. Popovic, B. Grzeta, B. Rakvin, E. Tkalcec, M. Vrankic, S. Kurajica, J. Alloys Compd., 509 (2011) 8487–8492.
[30] S. Ramachitra, R. Hema, P. Muthuausteria, K. Parthipan, J. Mol. Struct., 1058 (2014) 173–180.
[31] Santosh K. Gupta, R.M. Kadam, R. Gupta, Manjulata Sahu, V. Natarajan, Mater. Chem. Phys., 145 (2014) 162–167.
[32] Ram Kripal, M. Singh, Spectrochim. Acta. Part A, 135 (2015) 865–870.
[33] M. Acikgoz, P. Gnutek, Opt. Mater., 36 (2014) 1311–1318.
[34] Ram Kripal, Har Govind, Manisha Bajpai, Manju Maurya, Spectrochim. Acta. Part A, 71 (2008) 1302-1306.
[35] K. Ravindranadh, B. Babu, V. Pushpa Manjari, G. Thirumala Rao, M.C. Rao, R.V.S.S.N. Ravikumar, J. Lumin.159 (2015) 119–127.
[36] D.M. Wang, I. Kovacik, E.J. Reijerse, E.de Boer, Bull. Mag. Reson. 15,
[37] A. Abragam, B. Bleaney, Electron Paramegnetic Resonance of Transition Ions, Clarendon Press, Oxford, 1970.
[38] P. Sambasiva Rao, S. Subramanian, Mol. Phys. 54 (1985) 429-438.
[39] A. Forman, J.A. van Wyke, Can. J. Phys. 45 (1967) 3381-3386.
[40] P. Chand, C.G.J.Upreti, Chem. Phys. 81 (1984) 1650-1654.
[41] K.H. Kirklin, G.L.Mc Pherson, J. Phys. Chem 16 (1983) 6539-6550.
[42] M. Heming, G. Lehman, Phys. Status Solidi B, 124 (1984) 315-323.
[43] M. Korkmaz, M. Dupont, B. Aktas, J. Phys. Chem. Solids, 45 (1984) 465.
[44] B. Bleaney, R.S. Rubins, Proc. Roy. Soc. 77 (1961) 103-112.

IOSR Journal of Applied Physics (IOSR-JAP) is UGC approved Journal with Sl. No. 5010, Journal no. 49054.